VOLUMEN 37
XXX Verano De la Ciencia
ISSN 2395-9797
www.jovenesenlaciencia.ugto.mx

Segmentation and Classification of Magnetic Resonance Images

Segmentación y Clasificación de Imágenes de Resonancia Magnética

Alejandra Alfaro Flores[1], Laura Vanessa Montoya Agudelo[2], Luisa Fernanda Morales Zambrano[2], Fernando Daniel Hernandez-Gutierrez[1], Juan Gabriel Avina-Cervantes[1]

[1] Escuela de Nivel Medio Superior de Salamanca, División de Ingeniería del Campus Irapuato-Salamanca (DICIS), Universidad de Guanajuato.
[2] Universidad Simón Bolívar.
a.alfaroflores@ugto.mx, fd.hernandezgutierrez@ugto.mx, avina@ugto.mx, laura.montoya1@unisimon.edu.co, luisa.moralez@unisimon.edu.co

Abstract

Accurate diagnosis and early treating of brain tumors have a positive and significant impact on a person's quality of life. For this reason, several studies are currently being conducted to improve medical image processing and the detection and accurate localization of brain tumors. This has led to the implementation of Deep Learning (DL) in medical image analysis. Thus, this study presents a lightweight U-Net to reduce computational costs in the detection of brain tumors. This detection was performed by selecting the best slice from the Magnetic Resonance Images (MRI) of several modalities (T1C, T2W, and T2F) in the BrasTS2024 dataset. The proposed model automatically selects the best slice by extracting the slice with the major tumor content from the mask. An adaptive learning-rate scheduler was applied during training to ensure stable convergence. Among the modalities, T2W produced the best quantitative results, achieving a Dice coefficient of 0.760, an IoU of 0.623, and a sensitivity of 0.842. In contrast, T2F yielded visually comparable yet slightly lower metrics. These findings indicate that reducing model complexity needs not compromise accuracy and highlight the T2W sequence as the most informative single slice for tumor delineation.

Keywords: Brain Tumors; Convolutional Neural Networks; Lightweight U-Net; Semantic Segmentation; Magnetic Resonance Imaging.

Introduction

World Health Organization (WHO) has developed several studies finding that cancer has been responsible for approximately 9.7 million deaths per year (Canetta, 2021). Brain cancer accounts for 248,500 million deaths per year worldwide, ranking 12th among the different types of cancer in terms of mortality (World Health Organization, 2022). Brain tumors are abnormal masses of tissue characterized by the uncontrolled proliferation of cells (Jose *et al*., 2022). They originate in the spinal canal or brain (Moini *et al*., 2023). On one hand, brain tumors are classified into primary tumors, which originate directly in the brain and can be benign or malignant. On the other hand, metastatic tumors, which do not originate in the brain but spread to it through the bloodstream, are usually malignant (Goceri, 2025). Hence, the difference between benign and malignant tumors lies in their behavior; that is, the former is characterized by slow growth, generally has well-defined edges, and rarely spreads. Notably, malignant tumors are invasive and grow rapidly (American Brain Tumor Association, 2018). *Figure 1* presents the World Health Organization (WHO) classification system, which categorizes tumors into four distinct grades (Sinning, 2017).

Grade I	Tumors that grow slowly, do not become malignant and are generally associated with long-term survival of the patient.
Grade II	Tumors that grow slowly, do not become malignant and are generally associated with long-term survival of the patient.
Grade III	Tumors that grow actively. They often infiltrate adjacent brain tissue and generally become higher-grade tumors.
Grade IV	Tumors that grow rapidly and create blood vessels to continue their accelerated growth are malignant and create areas of dead cells (necrosis).

Figure 1. Tumor classification is based on grades.

Among the most common methods for diagnosing and monitoring tumors, Magnetic Resonance Imaging (MRI) plays a crucial role. Unlike computed tomography (CT) and X-rays, MRI allows us to visualize different organs and tissues in the body without the use of ionizing radiation. It generates magnetic fields and radio waves to obtain detailed images of the human body. This imagining technique is based on the mutual interaction between atomic nuclei and magnetic fields generated by the magnets of the magnetic resonator. This magnetic field causes the body's atoms to align in the same direction, and then radio waves are sent to displace these atoms from their original positions (Bangare, 2022). When the radio waves are turned off, the atoms return to their original positions, releasing energy that is captured and processed by a computer to produce an image of the anatomical region being examined (Carter *et al*., 2022). These images are obtainable through different weightings or sequences, which correspond to how the images are generated; the most common are T1 and T2 (Hattingen & Pilatus, 2016). For instance, T1-weighted images reflect the time it takes protons to return to their regular spin; this is achieved using short echo times (TE) and repetition times (TR), which creates images with high contrast between fat and water-rich tissue. By contrast, T2 images show the speed at which protons reach equilibrium or become out of phase using longer TE and TR times, thus producing images with high contrast between different types of fluids such as blood and cerebrospinal fluid, making it the most appropriate for identifying edema and lesions with high fluid content (Dhabalia *et al*., 2024). The advanced technology of MRI enables the characterization of four essential pathophysiological characteristics that define a brain tumor (Martucci *et al*., 2023): aggressiveness, cellularity, metabolism, and vascularization. The preceding, in turn, reassures us about the effectiveness of MRI in monitoring tumor progression or response to treatment.

Although advances in MRI imaging enable detailed visualization of the body's tissues and organs, interpretation remains subject to expert diagnosis. In this sense, image segmentation has become one of the most crucial steps in medical imaging studies and analysis (Hernandez-Gutierrez *et al*., 2024). Over the last decade, image segmentation and classification processes have made significant contributions to tumor diagnosis, enabling this process to be performed automatically and efficiently. However, these types of algorithms have some drawbacks when processing images, including sensitivity to noise and low robustness. Consequently, in recent years, the use of Deep Learning (DL) techniques has been incorporated, as evidenced by improvements in the results obtained compared to classical segmentation methods. In this context, they are used to estimate the location and size of brain tumors accurately. These algorithms mainly consist of convolutional networks with a U-shaped structure, known as UNet (Nizamani *et al*., 2023) (Wan *et al*., 2023). These have established themselves as one of the most effective methods in the field of medical image segmentation due to their structure, which includes an encoder block that extracts the most relevant features and a decoder block that reconstructs the image to its original size and already segmented (Nizamani *et al*., 2023).

Background

Currently, MRI techniques are being incorporated for the detection of brain tumors using artificial intelligence, deep learning, and Convolutional Neural Networks (CNNs). The aim is to achieve greater accuracy and reliability in the detection of brain tumors, which represents a significant advance in their diagnosis and treatment.

Kumar Sahoo *et al*. (2023) introduced a new model that segments and classifies images based on tumor type. It works in two stages. First, using a U-Net network with ResNet-18 on MRI t1-ce without processing, obtaining a 99.6% accuracy and 90.11% Dice score. In the Second stage, a YOLO2 transfer learning model was used to classify the segmented models, achieving 97% accuracy.

Additionally, Montaha *et al*. (2023) propose a model based on a U-Net architecture to segment brain tumors using 2D slices extracted from 3D images. They used the FLAIR, T1, T1ce, and T2 sequences from the BraTS 2020 dataset. The model used the Adam optimizer and a varied configuration of parameters. Its best performance was with the T1 sequence, with an accuracy of 99.41% and a DSC of 93.86%.

Two years ago, Wan *et al*. (2023) presented an advanced model for glioma segmentation on MRI, using Deep Learning techniques and multimodal data. RegNet is used to codify images, meanwhile DeepLasb3+ is used as a codifier. The model incorporates a composite loss function that enhances accuracy and reduces noise in the predictions. They used the LGG dataset and obtained a 94.36% Dice score.

Meanwhile, Muhammad Faheem Khan *et al*. (2024) introduced the OT model, a computer-aided system designed for the precise identification of brain gliomas. Significant preprocessing steps, including noise removal and tumor localization, significantly improved image quality, enabling accurate feature extraction. The OT model employed the Gray Level Co-occurrence Matrix for texture analysis and integrated a feature selection scheme to identify the thirty most relevant features, which were evaluated using three machine learning classifiers. The LSTM classifier achieved a classification accuracy of 83.71%, while the CNN classifier reached 84.50%.

Specifically, Hernandez-Gutierrez *et al*. (2024) developed a novel method for tumor segmentation based on an optimized U-Net, designed to segment the T2 sequence of MRI images automatically. The model includes a lightweight architecture with SELU activation functions and utilizes the SGD optimizer, trained in over 500 epochs. The BraTS 2017, 2020, and 2021 datasets were used for evaluation, with the best results achieved on the BraTS 2021 dataset. The outcomes demonstrated that the proposed model provides accurate segmentation while maintaining low computational requirements, making it ideal for devices with limited resources.

More recently, R Preetha and M (2025) proposed an advanced approach to brain tumor segmentation using a U-Net architecture with multiscale attention, integrating the EfficientNetB4 network as an encoder. This model enhances the extraction of hierarchical and contextual features at multiple scales, allowing for more accurate segmentation of tumor regions in MRI images. Additionally, spatial and channel attention mechanisms were incorporated to highlight relevant areas and suppress redundant information. The study demonstrated significant improvements in metrics such as Dice and IoU compared to conventional U-Net variants. However, it did not evaluate multi-class tasks or validate its results on heterogeneous clinical datasets.

Dorfner *et al*. (2025) explore advancements in deep learning for brain tumor analysis using MRI, emphasizing models such as U-Net, nnU-Net, and ResNet, which enhance tumor segmentation and classification with greater accuracy than traditional methods. These models also aid in predicting molecular biomarkers and monitoring treatment responses. While emerging techniques, such as vision transformers, show promise, challenges persist, including limited public datasets, demographic biases, concerns over generalizability and interpretability, as well as ethical issues in clinical implementation.

Finally, Revathi *et al*. (2025) proposed an advanced approach to brain tumor segmentation using a U-Net architecture with multiscale attention, integrating the EfficientNetB4 network as the encoder. This model enhances the extraction of hierarchical and contextual features at multiple scales, allowing for more accurate segmentation of tumor regions in MRI images. Additionally, spatial and channel attention mechanisms were incorporated to highlight relevant areas and suppress redundant information. The study demonstrated significant improvements in metrics, including Dice and IoU, compared to conventional U-Net variants. However, it did not evaluate multi-class tasks or validate on heterogeneous clinical datasets. *Table 1* summaries a comprehensive list of datasets and methodologies to detect brain tumors, which particularly use the BraTS datasets in recent literature.

Table 1. *Recent datasets and associated methods for brain tumor detection.*

Article	Dataset	Method	Year	Limitations
(Revathi *et al.*, 2025)	BraTS2020	DSCNN with Dense U-Net	2025	Inaccurate tumor boundary delineation, highly inefficient computationally, and challenges in managing diverse tumor types and sizes.
(Dorfner *et al.*, 2025)	BraTS, TCIA, CBTN	DL	2025	Currently, only a limited number of brain tumor-related models have been approved for clinical use in U.S.A.
(Preetha *et al.*, 2025)	Figshare	EfficientNetB4 with multi-scale Attention UNET model	2025	Lack of standardized comparison of inference time. Limited dataset diversity, absence of multi-class evaluation, and limited interpretability, as well as clinical validation of the model.
(Hernandez-Gutierrez *et al.*, 2024)	BraTS2017, BraTS2020, BraTS2021	Lightweight UNET	2024	Dataset's limited size and highly demanding computational resources.
(Muhammad Faheem Khan *et al.*, 2024)	LGG Segmentation	CNN	2024	Reduced reach of the proposed model and the need for a better method of detection. The use of Dice score as a metric of evaluation does not result in an appropriate measure of noise presence. Finally, the effect of other data modalities on the results obtained was not sufficiently analyzed.
(Wan *et al.*, 2023)	LGG Segmentation Dataset	DeepLabv3+ RegNet	2023	Noise detection function, as this is limited to binary and 2D segmentation. Although DICE is effective for quantifying similarities, it is not sufficiently informative in evaluating noise removal.
(Montaha *et al.*, 2023)	BraTS2020	UNET + resnet18	2023	Not enough number of images. In this regard, other 3D brain MRI datasets can be explored. Deep learning architecture can be further optimized with a hybrid approach that incorporates CNNs or attention mechanisms.
(Kumar Sahoo *et al.*, 2023)	Figshare	DL	2023	They focus solely on T1-CE images. Furthermore, by not utilizing the preprocessing stage to minimize computational load, limitations arise in terms of sensitivity, robustness against tumor variability, and the use of multimodal data.

Objectives

To adapt and rigorously evaluate a computationally efficient variant of the baseline U-Net architecture, obtained through targeted structural modifications, that delivers high-precision segmentation of intracranial tumors on magnetic resonance imaging (MRI) and establishes a solid foundation for its future deployment on resource-constrained embedded systems.

Specific Aims:

- Undertake an exhaustive critical review of current brain-tumor segmentation methodologies, with particular emphasis on U-Net and its lightweight derivatives, to distill state-of-the-art techniques for parameter compression, including depthwise separable convolutions, network pruning, and post-training quantization.
- Modify the standard U-Net by incorporating efficiency-oriented modules, such as pointwise and depthwise convolutional blocks, and streamlined residual pathways, with the dual aim of substantially reducing the parameter count and floating-point operations while preserving the capacity for contextual feature representation.
- Implement a systematic hyperparameter-tuning strategy that encompasses learning-rate scheduling, regularization techniques, and optimizer selection to maximize segmentation accuracy, quantified via the Dice similarity coefficient and Intersection over Union, under stringent computational constraints.

- Quantitatively assess the proposed lightweight model on established benchmark datasets, such as the BraTS series, using standard metrics (Dice, Intersection over Union, precision, and recall), and conduct comparative analyses against the unmodified U-Net and other contemporary lightweight baselines to determine its relative efficacy.

Methodology

Dataset

The BraTS2024 datasets comprise images acquired using multiparametric magnetic resonance imaging (mpMRI) protocols, including the following MRI sequences: T1-weighted without contrast (T1), T1-weighted with contrast (T1-Gd), T2-weighted (T2), and T2-weighted with fluid-attenuated inversion recovery (FLAIR). The data was obtained by seven academic medical centers (see *Figure 2*), where approximately 2,200 different cases were obtained. This database focuses on post-treatment MRIs of low- and high-grade diffuse gliomas (Correia de Verdier *et al*., 2024).

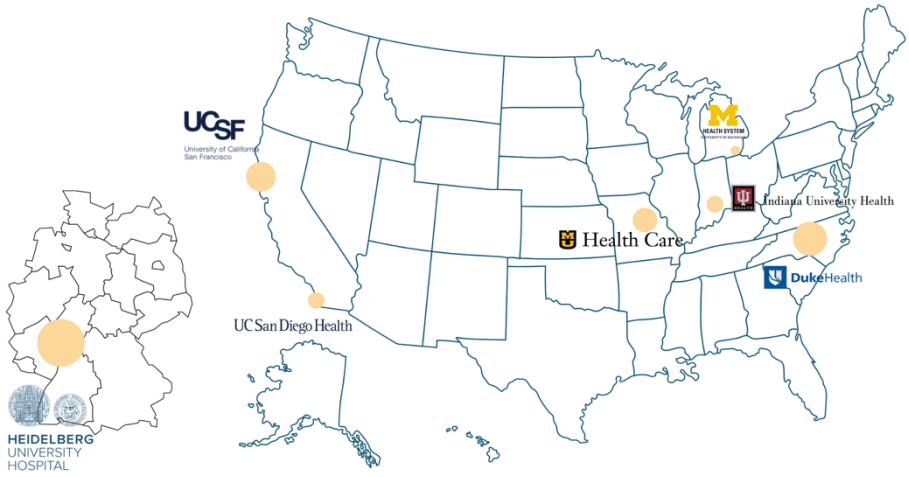

Figure 2. *Medical institutions from USA and Germany that contributed with data to build the 2024 Brain Tumor Segmentation dataset (BraTS2024).*

To obtain these images, software was applied to different sequences to convert the image format to the Neuroimaging Informatics Technology Initiative (NIfTI) file format (Correia de Verdier *et al*., 2024).

Function Loss

When segmenting medical images, we encounter various challenges related to the dataset, such as imbalance, as well as the complexity involved in segmenting a small portion of the image compared to its overall background (Yeung *et al*., 2022). This phenomenon, known as class imbalance, can impact the model's learning process, leading to bias and suboptimal segmentation performance. In semantic segmentation, particularly in binary segmentation, we find two main loss functions that are commonly used for this purpose. The first function is Binary Cross-Entropy (BCE), which measures the discrepancy between the ground truth and the model prediction in terms of the number of pixels. BCE is primarily used when the data is balanced, as it evaluates pixels independently without considering the relative proportions of foreground and background regions (Ma *et al*., 2024). The BCE function is defined as

$$\mathcal{L}_{BCE} = -\frac{1}{N}\sum_{i=1}^{N}[y_i \log(\hat{y}_i) + (1-y_i)\log(1-\hat{y}_i)] \quad (1)$$

Where N represents the number of samples, y_i represents the true label of the pixel, and $\hat{y}_i$ is the predicted probability that pixel belongs to the positive class.

Similarly, the DiceLoss function is used in image segmentation to evaluate class-imbalanced datasets (Hernandez-Gutierrez *et al*., 2025). It is a function described as

$$\mathcal{L}_{Dice} = 1 - 2\frac{\sum_{i=1}^{N} y_i \hat{y}_i}{\sum_{i=1}^{N} y_i + \sum_{i=1}^{N} \hat{y}_i} \quad (2)$$

Where N is the total number of pixels in the image, y_i represents the ground truth label and $\hat{y}_i$ corresponds to the predicted probability for each pixel.

Overall framework

In this study, a 70:15:15 split was chosen for training, validation, and testing (see *Figure 3*Figure 1). This percentage enables the model to learn tumor characteristics in a representative manner from MRI. It also focused on T2-Weighted images with fluid-attenuated inversion recovery (FLAIR), as these allow for better visualization of the tumor compared to the T1 sequence, while significantly reducing noise, unlike the T2 sequence. These differences can be better visualized in *Figure 4*Figure 4.

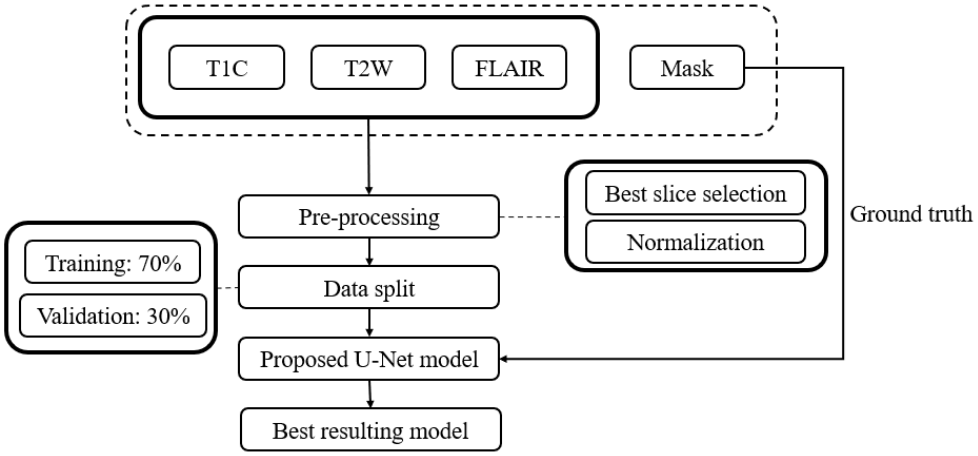

Figure 3. *Framework of the proposed tumor segmentation.*

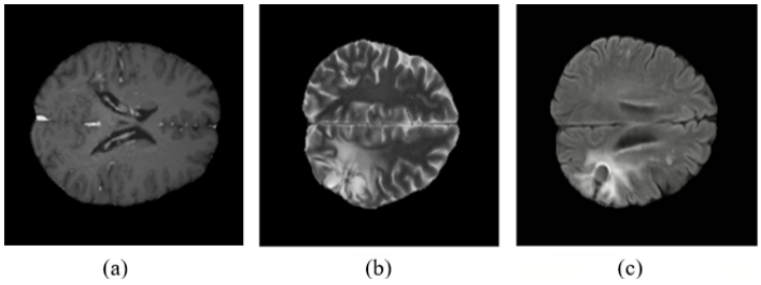

Figure 4. *Contrast difference between the Resonance Magnetic Images (MRI). (a) T1C, (b) T2W, and (c) T2F sequences.*

Preprocessing

For image preprocessing, the image was cropped into portions, and the one containing the highest percentage of the tumor was selected. Subsequently, the images were converted to grayscale. From among them, the one showing the most significant part of the tumor was selected to obtain a better visualization of segmentation. The resulting dataset was normalized and then resized to 240 x 240 pixels. Finally, a percentage of the dataset was assigned for training and another percentage for validation. This was done to optimize machine learning and improve the quality of the results.

Proposed model

The proposed model is based on a modified U-Net structure. It is a Lightweight U-Net architecture used in medical image segmentation tasks, as it helps reduce computational costs. It is a structure that has an encoder-decoder network. The encoder part oversees the extraction of relevant features using two layers of convolutions and max pooling operations, while the decoder part reconstructs the segmented mask using transposed convolutions. In addition, the connections between the layers allow for preserving spatial and edge information during the reconstruction process. For each layer, the SeLU activation function was used, along with batch normalization, which helped stabilize the training.

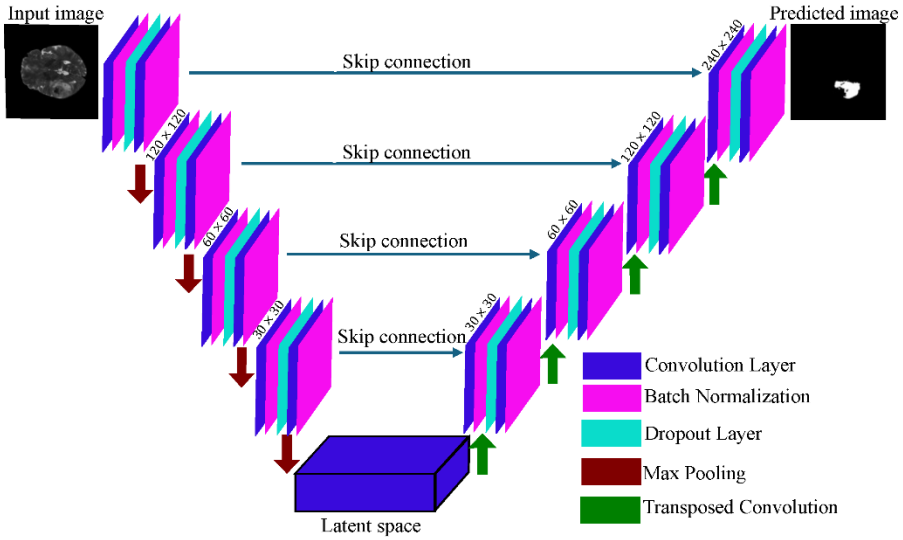

Figure 5. Modified UNET network architecture.

Results

This section details the segmentation results, and the evaluation metrics employed to assess the Lightweight U-Net on the BraTS 2024 dataset. The sequences evaluated were T1C, T2W, and T2-FLAIR (T2F). Each of them was set to 1000 epochs. The Binary Cross-Entropy Loss (BCE Loss) function was applied to all three sequences, and in the case of T2F, BCE-Dice Loss was also used to compare the effects on segmentation. A learning rate of 0.0001 was set. The results (prediction) were compared with the corresponding ground truth.

Evaluations Metrics

In this study, model performance is assessed with four key metrics: Dice Similarity Coefficient (DSC), Intersection over Union (IoU), precision, and sensitivity.

Dice Similarity Coefficient (DSC)

The Dice Similarity Coefficient (DSC) indicates the degree of overlap between the actual mask and the model's prediction. For this metric, the closer to 1, the more accurate the segmentation will be (Zanddizari *et al*., 2021). DSC is described by

$$DSC = 2\sum\frac{A \cap B}{A \cup B}, \tag{3}$$

Where A is a segmented imagen, and B represent the ground truth.

Intersection Over Union (IoU)

Like DSC, but more accurate. Intersection Over Union (IoU) evaluates the level of overlap between the ground truth and the model's prediction (Mohammed *et al*., 2024). IoU is mathematically defined by

$$Mean\ IoU = \sum \frac{A \cap B}{A \cup B} \tag{4}$$

Here *A* represents the ground-truth imagen, while *B* represents the predicted segmentation A ∩ B represent the overlap between two images

Precision

*Precision i*ndicates the model's accuracy in avoiding false positives; the higher the value obtained, the better (Peng *et al*., 2024).

$$Precision = \frac{|TP|}{|TP| + |FP|}, \tag{5}$$

TP represents the true positives, while FP represents the false positives.

Sensitivity (Recall)

Sensitivity (the recall score or true positive rate) corresponds to the model's ability to obtain the most significant amount of the tumor from the ground truth. The higher the sensitivity, the fewer omissions of true positives (Zhuang *et al*., 2021). Sensitivity is computed by

$$Sensitivity = \sum \frac{A \cap B}{B} \tag{6}$$

Segmentation Results

Figure 6 provides a qualitative comparison of the three MRI modalities. The left column contains the original slice, the center column shows the ground-truth mask, and the right column displays the model's prediction. The T2F sequence yields the most accurate delineation, as its lower cerebrospinal fluid (CSF) signal suppresses noise and enhances the contrast between the tumor and surrounding parenchyma, leading to a near-perfect overlap with the reference mask. The model's output for the T2W sequence is reasonably close to the ground truth, but residual intensity similarities between tumor and adjacent tissue cause mild over-segmentation. By contrast, the network fails to identify the lesion in the T1C sequence, resulting in an empty mask with no voxels labeled as a tumor.

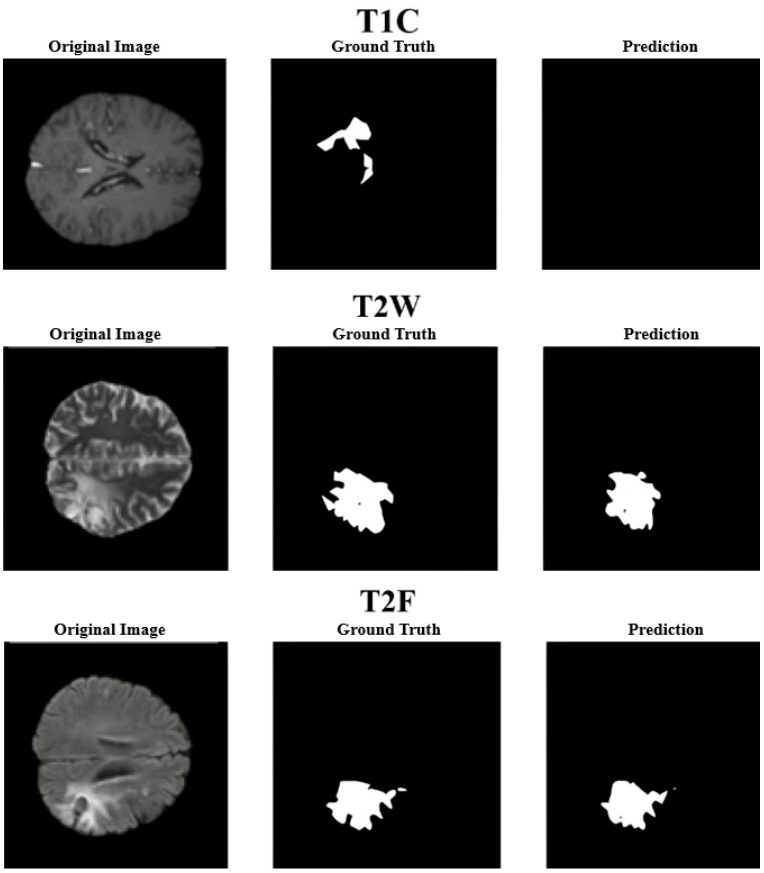

Figure 6. Brain tumor segmentation results using the BraTS 2024 dataset and BCELoss function.

Figure 7. Brain tumor segmentation results using the BraTS 2024 dataset and BCEDiceLoss function.

Evaluation metrics were computed separately for the three MRI modalities: T1C, T2W, and T2-FLAIR. For the contrast-enhanced T1 sequence (T1C), the model achieved a Dice similarity coefficient of 0.468, an IoU of 0.318, an accuracy of 0.849, and a sensitivity of 0.340. Although the accuracy appears high, the low Dice and IoU scores indicate minimal spatial overlap between the predicted mask and the ground truth. Visual inspection confirms that the network produced an essentially empty segmentation, suggesting that the T1C sequence does not provide sufficient tumor–background contrast for reliable delineation.

The T2W modality achieved the strongest quantitative performance across all sequences. It recorded a Dice similarity coefficient of 0.760 and an IoU of 0.623, indicating substantial spatial agreement between the predicted and ground-truth masks. Sensitivity was likewise highest, confirming that the network detected most tumor voxels. By contrast, overall accuracy was lower at 0.711, a decline likely attributable to the elevated cerebrospinal fluid (CSF) signal in T2W images, which introduces considerable visual noise and affects background classification.

The T2-FLAIR modality also demonstrated strong performance. When the model was trained with binary cross-entropy (BCE) loss, it achieved a Dice similarity coefficient of 0.707 and an IoU of 0.575. Replacing BCE with the combined BCE-Dice loss further raised the Dice score to 0.718, while the IoU remained comparable at 0.570. The combined loss function also produced higher overall accuracy, suggesting better identification of tumor voxels. Qualitative inspection in *Figure 7*, however, shows that the mask generated with BCE-Dice loss is more fragmented, whereas the mask obtained with BCE loss appears almost fully contiguous with the ground truth.

Table 2. *summarizes the data obtained for each of the sequences evaluated using the model.*

Table 2. Metrics obtained for each MRI sequence in the tumor detection process.

Sequence	Loss function	Dice	IoU	Precision	Sensitivity (Recall)
T1C	BCELoss	0.468	0.318	0.849	0.340
T2W		0.760	0.623	0.711	0.842
T2F		0.707	0.575	0.899	0.618
	BCEDiceLoss	0.718	0.570	0.903	0.609

Conclusions

This study presents a lightweight U-Net variant with optimized convolutional blocks for fully automated brain tumor segmentation. The most favorable results were obtained for the T2-weighted sequence trained with Binary Cross-Entropy (BCE) loss, yielding Dice = 0.760, IoU = 0.602, accuracy = 0.711, and sensitivity = 0.842. For the T2-FLAIR sequence, BCE produced Dice = 0.707, IoU = 0.575, precision = 0.899, and sensitivity = 0.618, whereas the combined BCE-Dice loss marginally increased Dice (0.718) and precision (0.903) but reduced sensitivity to 0.609.

These results indicate that the T2-weighted sequence with BCE maximizes sensitivity, while the T2-FLAIR sequence with BCE–Dice achieves the most balanced overall performance. The proposed architecture, therefore, delivers competitive segmentation accuracy with minimal computational overhead**.**

References

American Brain Tumor Association. (2018). *About Brain Tumors a primer for patients and caregivers*. American Brain Tumor Association. https://www.abta.org/wp-content/uploads/2018/03/about-brain-tumors-a-primer-1.pdf

Bangare, S. L. (2022). Classification of optimal brain tissue using dynamic region growing and fuzzy min-max neural network in brain magnetic resonance images. *Neuroscience Informatics*, *2*(3), 100019. https://doi.org/https://doi.org/10.1016/j.neuri.2021.100019

Canetta, E. (2021). Current and Future Advancements of Raman Spectroscopy Techniques in Cancer Nanomedicine. *International Journal of Molecular Sciences*. https://doi.org/10.3390/ijms222313141

Carter, M., Essner, R., Goldstein, N., & Iyer, M. (2022). Chapter 1 - Noninvasive Brain Imaging. In M. Carter, R. Essner, N. Goldstein, & M. Iyer (Eds.), *Guide to Research Techniques in Neuroscience (Third Edition)* (pp. 1–38). Academic Press. https://doi.org/https://doi.org/10.1016/B978-0-12-818646-6.00011-7

Correia de Verdier, M., Saluja, R., Gagnon, L., LaBella, D., Baid, U., Hoda Tahon, N., Foltyn-Dumitru, M., Zhang, J., Alafif, M., Baig, S., Chang, K., D'Anna, G., Deptula, L., Gupta, D., Ammar Haider, M., Hussain, A., Michael, I., Kontzialis, M., Manning, P., … Rudie, J. D. (2024). The 2024 Brain Tumor Segmentation (BraTS) Challenge: Glioma Segmentation on Post-treatment MRI. *ArXiv E-Prints*, arXiv:2405.18368. https://doi.org/10.48550/arXiv.2405.18368

Dhabalia, R., Kashikar, S., Parihar, P., & Mishra, G. (2024). Unveiling the Intricacies: A Comprehensive Review of Magnetic Resonance Imaging (MRI) Assessment of T2-Weighted Hyperintensities in the Neuroimaging Landscape. *Cureus*, *16*. https://doi.org/10.7759/cureus.54808

Dorfner, F. J., Patel, J. B., Kalpathy-Cramer, J., Gerstner, E. R., & Bridge, C. P. (2025). A review of deep learning for brain tumor analysis in MRI. *Npj Precision Oncology*, *9*(1), 2. https://doi.org/10.1038/s41698-024-00789-2

Goceri, E. (2025). An efficient network with CNN and transformer blocks for glioma grading and brain tumor classification from MRIs. *Expert Systems with Applications*, *268*, 126290. https://doi.org/https://doi.org/10.1016/j.eswa.2024.126290

Hattingen, E., & Pilatus, U. (Eds.). (2016). *Brain Tumor Imaging: Vol. VII*. Springer Berlin Heidelberg. https://doi.org/10.1007/978-3-642-45040-2

Hernandez-Gutierrez, F. D., Avina-Bravo, E. G., Ibarra-Manzano, M. A., Ruiz-Pinales, J., Ovalle-Magallanes, E., & Avina-Cervantes, J. G. (2025). Retinal Vessel Segmentation Based on a Lightweight U-Net and Reverse Attention. *Mathematics*, *13*(13). https://doi.org/10.3390/math13132203

Hernandez-Gutierrez, F. D., Avina-Bravo, E. G., Zambrano-Gutierrez, D. F., Almanza-Conejo, O., Ibarra-Manzano, M. A., Ruiz-Pinales, J., Ovalle-Magallanes, E., & Avina-Cervantes, J. G. (2024). Brain Tumor Segmentation from Optimal MRI Slices Using a Lightweight U-Net. *Technologies*, *12*(10). https://doi.org/10.3390/technologies12100183

Jose, J., Bandiwadekar, A., Figreda, G. G., & Crasta, C. M. (2022). 14 - Dendrimers as carriers for active targeting of brain tumors. In L. Kumar & Y. Y. Pathak (Eds.), *Nanocarriers for Drug-Targeting Brain Tumors* (pp. 401–430). Elsevier. https://doi.org/https://doi.org/10.1016/B978-0-323-90773-6.00001-4

Kumar Sahoo, A., Parida, P., Muralibabu, K., & Dash, S. (2023). Efficient simultaneous segmentation and classification of brain tumors from MRI scans using deep learning. *Biocybernetics and Biomedical Engineering*, *43*(3), 616–633. https://doi.org/https://doi.org/10.1016/j.bbe.2023.08.003

Martucci, M., Russo, R., Schimperna, F., D'Apolito, G., Panfili, M., Grimaldi, A., Perna, A., Ferranti, A. M., Varcasia, G., Giordano, C., & Gaudino, S. (2023). Magnetic Resonance Imaging of Primary Adult Brain Tumors: State of the Art and Future Perspectives. *Biomedicines*, *11*(2). https://doi.org/10.3390/biomedicines11020364

Mohammed, S. A. K., Razak, M. Z. A., Rahman, A. H. A., & Bakar, M. A. (2024). An Efficient Intersection Over Union Algorithm for 3D Object Detection. *IEEE Access*, *12*, 169768–169786. https://doi.org/10.1109/ACCESS.2024.3495761

Montaha, S., Azam, S., Rakibul Haque Rafid, A. K. M., Hasan, Md. Z., & Karim, A. (2023). Brain Tumor Segmentation from 3D MRI Scans Using U-Net. *SN Computer Science*, *4*(4), 386. https://doi.org/10.1007/s42979-023-01854-6

Muhammad Faheem Khan, Arslan Iftikhar, Huzaifa Anwar, & Sadaqat Ali Ramay. (2024). Brain Tumor Segmentation and Classification using Optimized Deep Learning. *Journal of Computing & Biomedical Informatics*, *7*(01), 632–640. https://jcbi.org/index.php/Main/article/view/528

Nizamani, A. H., Chen, Z., Nizamani, A. A., & Bhatti, U. A. (2023). Advance brain tumor segmentation using feature fusion methods with deep U-Net model with CNN for MRI data. *Journal of King Saud University - Computer and Information Sciences*, *35*(9), 101793. https://doi.org/https://doi.org/10.1016/j.jksuci.2023.101793

Peng, M., Liu, Y., Qadri, I. A., Bhatti, U. A., Ahmed, B., Sarhan, N. M., & Awwad, E. M. (2024). Advanced image segmentation for precision agriculture using CNN-GAT fusion and fuzzy C-means clustering. *Computers and Electronics in Agriculture*, *226*, 109431. https://doi.org/https://doi.org/10.1016/j.compag.2024.109431

Preetha, R., Jasmine Pemeena Priyadarsini, M., & Nisha, J. S. (2025). Brain tumor segmentation using multi-scale attention U-Net with EfficientNetB4 encoder for enhanced MRI analysis. *Scientific Reports*, *15*(1), 9914. https://doi.org/10.1038/s41598-025-94267-9

R Preetha and M, J. P. P. and J. S. N. (2025). Brain tumor segmentation using multi-scale attention U-Net with EfficientNetB4 encoder for enhanced MRI analysis. *Scientific Reports*, *15*(1), 9914. https://doi.org/10.1038/s41598-025-94267-9

Revathi, K. G., Shirley, C. P., Sreethar, S., & P, E. (2025). Brain tumor segmentation using optimized depth wise separable convolutional neural network with dense U-Net. *Knowledge-Based Systems*, *324*, 113678. https://doi.org/https://doi.org/10.1016/j.knosys.2025.113678

Wan, B., Hu, B., Zhao, M., Li, K., & Ye, X. (2023). Deep learning-based magnetic resonance image segmentation technique for application to glioma. *Frontiers in Medicine*, *10-2023*. https://doi.org/10.3389/fmed.2023.1172767

World Health Organization. (2022). *Cancer Today*. https://gco.iarc.who.int/today/en/dataviz/pie?mode=population&group_populations=0&types=1&cancers=31

Zanddizari, H., Nguyen, N., Zeinali, B., & Chang, J. M. (2021). A new preprocessing approach to improve the performance of CNN-based skin lesion classification. *Medical & Biological Engineering & Computing*, *59*(5), 1123–1131. https://doi.org/10.1007/s11517-021-02355-5

Zhuang, Z., Yang, Z., Raj, A. N. J., Wei, C., Jin, P., & Zhuang, S. (2021). Breast ultrasound tumor image classification using image decomposition and fusion based on adaptive multi-model spatial feature fusion. *Computer Methods and Programs in Biomedicine*, *208*, 106221. https://doi.org/https://doi.org/10.1016/j.cmpb.2021.106221